Extrapolation of hadron production in nucleus-nucleus collisions to energies reached at the BNL Relativistic Heavy Ion Collider and CERN Large Hadron Collider with the two-component dual parton model

I. Kawrakov, H.-J. Möhring, and J. Ranft*

Fachbereich Physik, Universität Leipzig, Leipzig, Federal Republic of Germany

(Received 9 November 1992)

We present a Monte Carlo version of the dual parton model for the description of particle production in hadron-nucleus and nucleus-nucleus collisions. Each nucleon-nucleon collision is described by the two-component dual parton model. Soft hadronic collisions and hard perturbative collisions (minijets) are the two components included in the unitarization scheme. Depending on the transverse momentum cutoff we find up to several thousand minijets in collisions of heavy ions at the TeV energies of the future CERN Large Hadron Collider (LHC). We get predictions up to energies reached at the LHC for the rapidity and transverse momentum distributions and the minijet component of the hadronic energy density.

I. INTRODUCTION

Experiments at the proton-antiproton colliders did indicate that hard and soft production processes are closely related. The best known of these experiments is the observation of correlations between the average transverse momenta and the charged multiplicity of produced hadrons [1]. These experiments can be explained by perturbative hard or semihard constituent scattering. The same constituent scattering is also responsible for at least part of the rise of the hadronic cross sections with energy. This was studied within the framework of the dual parton model (DPM) [2] quantitatively in papers by Capella, Tran Thanh Van, and Kwiecinski [3], Durand and Pi [4], and more recently Engel, Bopp, Pertermann, and Ranft [5]. In these papers the consequences for the total and inelastic cross sections of the unitarization of soft and hard scattering cross sections were studied.

A full description of the two-component DPM incorporating soft hadronic processes, described by the supercritical Pomeron, and semihard processes, described by perturbative constituent scattering, was given by Aurenche *et al.* [6]; see also [7,8]. The model for hadron-hadron collisions is implemented in the form of the dual parton model Monte Carlo code DTUJET.

The dual parton model for processes with nuclear targets and projectiles, in the approximation with only single Pomeron exchange in each elementary hadron-nucleon collision in the nucleus and with a full formation zone intranuclear cascade has been compared recently to data from hadron-nucleus and nucleus-nucleus collisions [9,10]. This model is implemented in the event generator DTUNUC, version 1.0 [11] and version 1.1 [12].

Here we use the combined model, which implements in each hadron-nucleon collision inside the nucleus multiple soft and hard chains such as in hadron-hadron collisions as described by the two-component dual parton model

[6]. This Monte Carlo event generator is implemented in the code DPMJET. In addition to multiple soft and hard chains, like in the DTUJET Monte Carlo program, DPMJET uses the Glauber model cascade in the formulation of Shmakov, Uzhinnski, and Zadorozhnyi [13]. The multiparticle chains are fragmented using the BAMJET independent chain decay code [14].

Furthermore, DPMJET has the following features. (i) A full formation zone suppressed intranuclear cascade is handled like in DTUNUC; i.e., all generations of secondary interactions with spectator nucleons are considered (in contrast with Refs. [15] where only the first generation was taken into account). It should, however, be noted that this feature plays no role in central nucleus-nucleus collisions, where practically no spectators are left. (ii) Fermi momenta of nucleons within the interacting nuclei are introduced, together with a simple realization of Pauli's principle. (iii) To allow for the application of the model at superhigh energies a parametrization for the energy dependence of the scattering amplitude (used in the Glauber formalism) is introduced.

DPMJET can be used up to energies reached at the CERN Large Hadron Collider (LHC) to sample hadron-hadron, hadron-nucleus, and normal and central nucleus-nucleus collisions according to the dual parton model. For hadron-hadron collisions, the results from DPMJET agree with the ones obtained with DTUJET [6].

In Sec. II we describe the two-component dual parton model in nuclear collisions. In Sec. III we present the resulting hadron production in central nucleus-nucleus collisions at energies reached at the BNL Relativistic Heavy Ion Collider (RHIC) and LHC. In Sec. IV the partonic (minijet) component of the hadronic energy density is discussed and in Sec. V we give a summary.

II. THE TWO-COMPONENT DUAL PARTON MODEL IN HADRON-NUCLEUS AND NUCLEUS-NUCLEUS COLLISIONS

We have experienced, in the dual parton model, that the approximation of *independent production and frag-*

*Address after March 31, 1993: Tarostrasse 13/905, D-0-7010 Leipzig, Germany.

mentation of multiparticle chains agrees very well with experimental data. In antiproton-proton collisions, this has been checked up to the c.m. system (c.m.s.) energy of 1.8 TeV [6]. In hadron-nucleus and nucleus-nucleus collisions this has been checked up to S-Pb collisions with 200 GeV per nucleon [9,10,15]. We expect that this independent production and fragmentation of strings will eventually break down at high energies, high spatial densities of the strings, and high hadronic energy densities. The new physics which will take over might be the interaction or fusion of hadronic chains [16] or the formation of a quark-gluon plasma [17]. In the present paper we extrapolate the independent production and fragmentation of strings up to the highest energies and energy densities. The deviation of experimental results from these predictions would be a clear signal for a new dynamics taking over. In this section we give an account on our formulation of the Glauber cascade and of the two-component dual parton model in each hadron-hadron subcollision. Both topics are described in more detail in Refs. [9,10,15] and [6].

A. The Glauber cascade

The starting point of our model is a frozen discrete spatial configuration of nucleons sampled from standard density distribution. The interaction proceeds via n elementary collisions between n_p and n_t nucleons from the projectile and the target nucleus, respectively. The numbers n, n_p, n_t are sampled according to Glauber's multiple scattering formalism in the Monte Carlo formulation of Ref. [13]. Particle production in each elementary nucleon-nucleon collision is described as in hadron-hadron interactions. From the Glauber cascade and the two-component dual parton model for the hadron-nucleon collision the chain structure of the event is fixed. The chains are fragmented into pseudoscalar and vector mesons and octet and decuplet baryons using the chain decay code BAMJET [14].

The decay of the hadronic resonances is done by the code DECAY [18].

Extrapolation to very high energies. Energy-dependent quantities enter the Glauber approach via the profile function of elastic hadron-nucleon scattering:

$$\gamma_{hN}(b) = \frac{1}{2\pi i p} \int d^2q \, \exp(i\mathbf{q}\cdot\mathbf{b}) f_{hN}(\mathbf{q}) , \qquad (2.1)$$

i.e., the amplitude of elastic hadron-nucleon scattering in the impact parameter representation (with $\mathbf{q}$ denoting the lateral, i.e., two-dimensional, momentum transfer). In their Monte Carlo realization of Glauber's approach Shmakov, Uzhinskii, and Zadorozhnyi [13] apply the high-energy approximation of the profile function:

$$\gamma_{hN}(b) = \frac{\sigma_{hN}^{\text{tot}}}{4\pi a} \left[1 - i \frac{\mathrm{Re} f_{hN}(0)}{\mathrm{Im} f_{hN}(0)} \right] \exp\left[-\frac{b^2}{2a} \right] , \qquad (2.2)$$

with parameters σ^{tot}, a, and $\rho = \mathrm{Re} f_{hN}(0)/\mathrm{Im} f_{hN}(0)$ appropriate for the description of nucleus-nucleus interactions at energies of several GeV per nucleon. [The parametrization (2.2) corresponds to a differential cross sec-

tion $d\sigma/dt \simeq \sigma_{\text{tot}} \exp(a \cdot t)$ with $t \simeq -\mathbf{q}^2$.]

However, the energy dependence of the elastic hadron-nucleon scattering amplitudes will influence the properties of hadron- (nucleus-) nucleus scattering. In particular, the number of individual high-energy hadron-nucleon interactions (n, n_p, n_t) will increase with rising energy; hence, the multiplicity will increase stronger than to be expected from the energy dependence of single hadron-hadron interactions.

Guided by the data collected in Ref. [19], we apply the following parametrizations for the slope parameter a: $a = 8.5 \, (1 + 0.065 \ln s)$ for nucleon-nucleon collisions and $a = 6.0 \, (1 + 0.065 \ln s)$ for π- and K-nucleon collisions (a given in GeV^{-2}). We use for the ratio ρ of the real and imaginary part of the elastic scattering amplitude: $\rho = -0.63 + 0.175 \ln\sqrt{s}$ for the energy region $3.0 \le \sqrt{s} \le 50$ and $\rho = 0.1$ in the energy region $\sqrt{s} \ge 50$ GeV in nucleon-nucleon scattering and $\rho = 0.01$ for π- and K-nucleon scattering.

The energy dependence of the total cross sections is described by the fits of the Particle Data Group [20]; at energies beyond the range of the actual parametrization of the pp cross section the one for $\bar{p}p$ is applied and at energies even higher we use the total cross sections as calculated by the dual parton model for hadron-hadron collisions [6].

B. The two-component dual parton model

The two-component dual parton model for hadron-hadron collisions contains two parts: a soft component described by the supercritical Pomeron and the hard component described by perturbative QCD which we call the hard Pomeron. Further components, which we will not describe here, are low-mass and high-mass single and double diffraction; see [6].

In the considered energy range, soft hadron-hadron interaction is dominated by s-channel iterated soft Pomeron exchanges. The individual Pomeron exchange which builds up this iteration can be parametrized as (supercritical Pomeron)

$$\sigma_s = g^2 s^{\alpha - 1} , \qquad (2.3)$$

where g^2 is a normalization constant and α the intercept of the Pomeron trajectory. This cross section increases with energy and, taken by itself, violates the unitarity bound.

If not merely absorptive, a Pomeron is *cut* which means that it contributes to the production of two chains (or strings) of produced particles. These chains are "stretched" between constituents of the incoming hadrons. For the simplest, the one-cut Pomeron case, the constituents of the proton are one-valence quark and one-valence diquark. The slightly more complicated two-cut Pomeron is given in Fig. 1. Here the hadron constituents also include sea quarks. Cutting an additional Pomeron we get two new chains and new sea quarks at the ends of chains.

Perturbative QCD predicts a hard component which with increasing energies plays a more and more significant role and therefore has to be included in
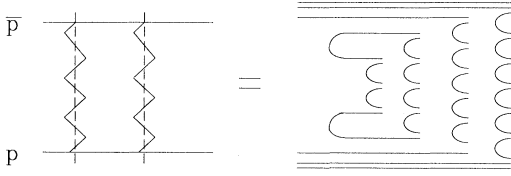
FIG. 1. The two-cut soft Pomeron graph producing four chains.

FIG. 2. The four-chain contribution to a semihard scattering.

minimum bias models. In the present model [6] the hard cross section σ_h is calculated with a lower transverse momentum cut $p_\perp^{\text{cutoff}} = 3$ GeV/c. To calculate the hard cross section we apply lowest-order QCD [21] and use conventional structure functions [22]. The result is shown in Table I. The hard cross section increases with energy practically as a power of s. The necessity of unitarization is even more manifest.

In Fig. 2 we give an example how a hard component contributes to the chain production. Ignoring color combinatorics the picture is as follows. Two gluons undergo a hard $2 \rightarrow 2$ scattering and the final state gluons, which have transverse momenta $p_\perp \geq p_\perp^{\text{cutoff}}$, are split into quark-antiquark pairs. These quarks and antiquarks sit at the ends of two chains. To neutralize the colors of the gluons removed by the hard scattering two spectator chains are exchanged in addition to the *hard* ones. The splitting function was chosen extremely asymmetrical; in the interesting region practically only one hard jet contributes for each hard scattering.

The soft and hard scattering are independent of each other except for their sharing the energy and momentum of the incoming hadrons.

In the Appendix we give technical details about the

TABLE I. Cross sections for the hard scattering of constituents with lower $p_\perp$ cutoffs $p_{\perp\text{thr}} = 2$ and 3 GeV/c calculated with parton distributions according to Martin, Roberts, and Stirling [22] with $\Lambda = 0.107$ GeV.

$\sqrt{s}$ (TeV)	σ_h (mb)$p_{\perp\text{thr}} = 2$ GeV/c	σ_h (mb)$p_{\perp\text{thr}} = 3$ GeV/c
0.005	1.1×10^{-8}	
0.01	1.4×10^{-3}	7×10^{-6}
0.02	0.099	4.7×10^{-3}
0.035	0.58	0.058
0.053	1.48	0.196
0.1	4.22	0.73
0.2	9.76	2.02
0.35	16.6	3.79
0.54	23.7	5.72
1	36.7	9.53
2	56.4	15.7
5	91.5	27.8
10	126.3	40.9
20	168.3	57.8
40	219.3	79.3
100	301	116
200	375	158

two-component dual parton model and the unitarization procedure. In the unitarization procedure we calculate, in addition to the total, elastic, and similar cross sections, also the exclusive cross sections for multi-Pomeron exchange. The cross sections for events with l_c soft and m_c hard scattering processes are calculated with a unitary scheme which is a generalization of the eikonal one, in which the Abramovskii-Gribov-Kancheli (AGK) cutting rules [23] are satisfied:

$$\sigma(l_c, m_c, B, s) = \frac{(2\chi_s)^{l_c}}{l_c!} \frac{(2\chi_h)^{m_c}}{m_c!} e^{-2\chi(B,s)} . \quad (2.4)$$

The average multiplicities of hard and soft scattering processes, which follow from this, increase with energy and at highest energies a sizable part of events has more than one hard or soft scattering.

The partons at the ends of the hard chains get transverse momenta $p_\perp \geq p_\perp^{\text{cutoff}}$ as predicted by perturbative QCD [7]. It is also reasonable to give some *soft* transverse momenta to the partons at the ends of the chains resulting from the cut soft Pomerons.

We take the point of view and assume that the subdivision of multiparticle chains into *soft* and *hard* ones is only due to our inability to solve QCD at low $p_\perp$. We therefore expect to get a continuous transition from soft to hard jets. For this purpose we introduced a $p_\perp$ distribution for the partons at the ends of the soft chains, which matches the hard chain $p_\perp$ distribution at $p_\perp = p_\perp^{\text{cutoff}}$ as described in [6]. This continuity requirement gives to the soft chain ends sizable transverse momenta, which rise with the collision energy to values considerably bigger than typically soft ones. This procedure has advantages. It produces a smoother transverse momentum distribution. A smooth transverse momentum distribution is indicated by data which show no hint of a break in the typical range of the cutoff parameter.

C. Nuclear shadowing of minijets

For small x values the parton structure functions $f_A(x, Q^2)$ of nuclei are not additive in the nucleon number A. However, so far we have assumed $f_A(x, Q^2) = A f_N(x, Q^2)$. It has been determined experimentally, that the number of quarks and antiquarks in the nucleus is depleted in regions of low x [24]. We follow here the procedure used in [25] and describe the nuclear shadowing for quarks and gluons by the following expression proposed in Refs. [26,27]:

$$R_A(x) = \frac{f_A(x)}{Af_N(x)}$$

$$= 1 + 1.19\ln^{1/6}A\,[x^3 - 1.5(x_0 + x_L)x^2 + 3x_0 x_L x] - \left[\alpha_A - \frac{1.08(A^{1/3}-1)}{\ln(A+1)}\sqrt{x}\right]\exp\left[-\frac{x^2}{x_0^2}\right],$$

(2.5)

$$\alpha_A = 0.1(A^{1/3}-1),$$

with $x_0 = 0.1$ and $x_L + 0.7$. It was shown in [25] that this form agrees with the European Muon Collaboration (EMC) data [24].

III. EXTRAPOLATION OF HADRON PRODUCTION IN CENTRAL NUCLEUS-NUCLEUS COLLISIONS TO ENERGIES REACHED AT RHIC AND LHC

A. Properties of central nucleus-nucleus collisions

In order to discuss the A dependence of nuclear collisions it is sufficient to consider the simplified model with only single Pomeron exchange in the individual nucleon-nucleon interactions. In this case the rapidity distribution in nucleus-nucleus collision in the DPM is given by the equation [2]

$$\frac{dN^{AB}}{dy} = \frac{1}{\sigma^{AB}}\left[\sum_{n_p,n_t,n}\sigma^{AB}_{n_p,n_t,n}\theta(n_t-n_p)\{n_p[N^{qq_v^A-q_v^B}(y)+N^{q_v^A-qq_v^B}(y)]+(n_t-n_p)[N^{\bar{q}_s^A-q_v^B}(y)+N^{q_s^A-qq_v^B}(y)]\right.$$

$$\left. +(n-n_t)[N^{q_s^A-\bar{q}_s^B}(y)+N^{\bar{q}_s^A-q_s^B}(y)]\}+\mathrm{sym}(n_p\leftrightarrow n_t)\right].$$

(3.1)

Here, $\sigma^{AB}_{n_p,n_t,n}$ is the cross section for n inelastic nucleon-nucleon interactions involving n_p, n_t participants from the projectile nucleus A and target nucleus B, respectively, $\sigma^{AB} = \sum \sigma^{AB}_{n_p,n_t,n}$. We calculate them, as mentioned in Sec. I, according to the procedure of Ref. [13]. Their explicit analytic form can be found for example in Ref. [28]. The $N^{q-q}(y)$ stand for the inclusive spectra resulting from the various strings. In our Monte Carlo simulation we found that at low energies sea-sea chains are kinematically suppressed (see Fig. 3, where the number of Glauber collisions per nucleon is presented; the straight lines correspond to N/A as obtained in the Glauber cascade, the dotted lines represent N/A after rejection due to kinematics). Also, because of the x^{-1} dependence of the sea quark distribution functions, the invariant mass of sea-sea chains is small compared to the mass of valence chains (and therefore the number of particles from a sea-sea chain is small compared to the number of particles from a valence-valence chain). Therefore in a first approximation the contribution from the sea-sea chains can be neglected and we write

$$\left.\frac{dN^{AA}}{dy}\right|_{y=0} = \bar{n}_p \left.\frac{dN^{pp}}{dy}\right|_{y=0},$$

(3.2)

where $\bar{n}_p$ is the average number of participating projectile nucleons. Otherwise in the limit of very high energies, the difference between sea and valence chains becomes less and less important. In this case we get approximately

$$\left.\frac{dN^{AA}}{dy}\right|_{y=0} = \bar{n} \left.\frac{dN^{pp}}{dy}\right|_{y=0},$$

(3.3)

with $\bar{n}$ being the average number of inelastic nucleon-nucleon interactions. In the Glauber approximation, which we use to describe nucleus-nucleus collisions we
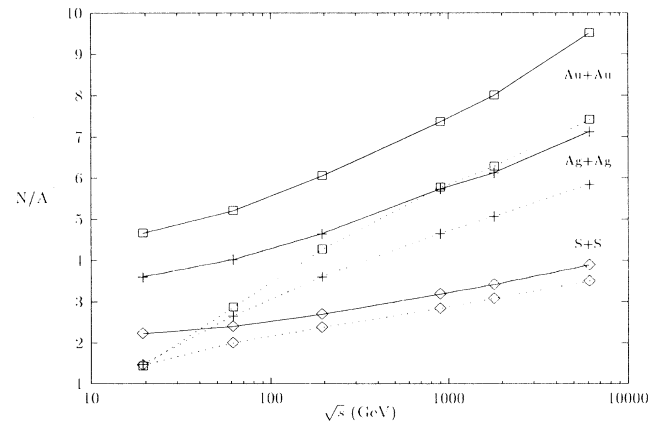

FIG. 3. The average number of elementary nucleon-nucleon interactions in central $A+A$ collisions as a function of the c.m.s. energy. The solid lines correspond to the numbers as required from the Glauber cascade, the dotted is the number of such interactions realized in the Monte Carlo simulation after rejection due to kinematics.

obtain for minimum bias events $\bar{n}_p \simeq c_1 A$ and $\bar{n} \simeq c_2 A^{4/3}$. The constants c_1 and c_2 depend on the particular choice of the nuclear density function and on the total nucleon-nucleon cross section. In central collisions, $n_p \simeq A$, but for the average number of inelastic nucleon-nucleon interactions $\bar{n}$, to our knowledge no analytic expression is known. Numerically it seems that $\bar{n}$ rises above $A^{4/3}$ as

$\sqrt{s} \to \infty$.

Let us now define the power α to describe the A dependence:

$$\alpha(s,y) = \ln \left[\frac{dN^{AA}/dy}{dN^{BB}/dy} \right] \Big/ \ln(A/B) . \qquad (3.4)$$

From the above discussion we have

$$\alpha(s,y=0) = \begin{cases} 1 & \text{low-energy limit, central and minimum bias ,} \\ 4/3 & \text{high-energy limit, minimum bias ,} \\ >4/3 & \text{high-energy limit, central .} \end{cases} \qquad (3.5)$$

We calculated $\alpha(s,y)$ from the results of our Monte Carlo model for minimum bias as well as for central collisions. In Fig. 4, $\alpha(s,y=0)$ is presented as a function of the c.m.s. energy per nucleon-nucleon in central and minimum bias events. In all calculations the standard Woods-Saxon density function and nuclei in the range $A = 32...197$ were used. As can be seen at $\sqrt{s} = 20A$ GeV the low-energy limit from Eq. (3.5) is satisfied. However, the high-energy limit seems not to be reached both in central and minimum bias collisions at the energy reached at LHC. In the projectile and target fragmentation regions, less particles per colliding nucleon are produced in nucleus-nucleus collisions than in pp collisions due to energy conservation. This effect, called nuclear attenuation, was observed experimentally already in pA interactions. In Fig. 5, $\alpha(s,y)$ is presented as a function of y at $\sqrt{s} = 200A$ GeV and $\sqrt{s} = 6300A$ GeV. As can be seen $\alpha(s,y \to y_{max}) \simeq 0.7$ (in this limit it is of course better to plot α as a function of Feynman x_F).

Because of the combinatorics of the chain ends and multiple Pomeron interactions, the importance of sea-sea and sea-valence chains increases strongly with increasing energy and nuclear number, reducing the number of

valence-valence chains. This feature of our model is demonstrated in Fig. 6, where the chain mass distribution in $p+p$ and central $S+S$ and $Au+Au$ collisions at $\sqrt{s} = 200$ and $\sqrt{s} = 6100$ GeV per nucleon-nucleon is presented. The thick lines correspond to the chain mass distribution of all chains (valence-valence, sea-valence and valence-sea, sea-sea, minijets) and the thin lines to
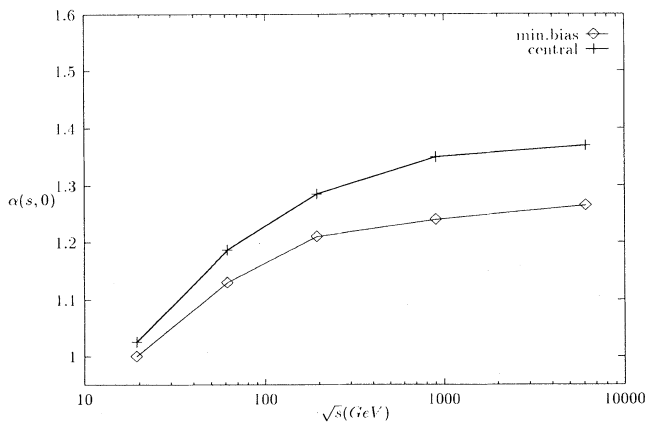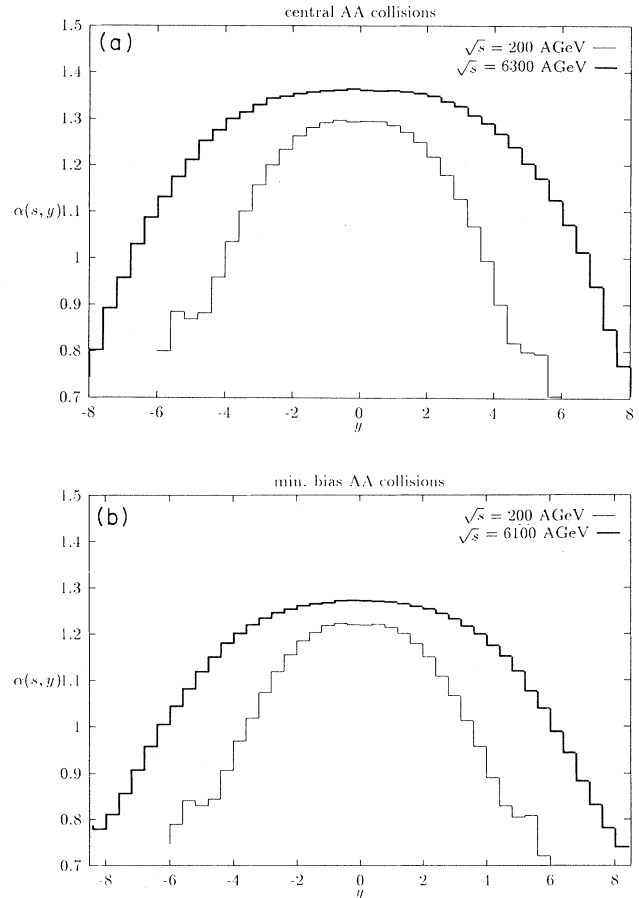
FIG. 4. $\alpha(s,y=0)$ as defined in Eq. (3.4) as a function of the c.m.s. energy per nucleon-nucleon, calculated from dN^{AA}/dy in central and minimum bias AA collisions in the range $A = 32–197$.

FIG. 5. $\alpha(s,y=0)$ as defined in Eq. (3.4) as a function of the rapidity y at $\sqrt{s} = 200A$ GeV (thin line) and $\sqrt{s} = 6300A$ GeV (thick line), calculated from dN^{AA}/dy in (a) central and (b) minimum bias AA collisions in the range $A = 32–197$.

the distribution of sea-sea chains. The small bend in the total distribution at $M = 6$ GeV/c^2 that can be seen at the energy reached at LHC is due to the contribution of minijets (remember that the calculations were carried out with a $p_\perp^{\text{cutoff}} = 3$ GeV/c; this corresponds to a minimal mass of 6 GeV/c^2 of the hard chains).

Finally we present in Fig. 7 the fraction of particles resulting from the fragmentation of minijets to the total particle number. As can be seen, even at energies reached at LHC only 10% of the particles produced in central nucleus-nucleus interactions result from minijets. We want to note here that in all simulations the Martin-Roberts-Stirling set 1 (MRS-1) structure functions [22] with x^{-1} behavior were used to calculate the cross section for hard Pomeron exchange. The authors of Ref. [8] found, studying the influence of the structure functions on the particle production in $p\bar{p}$ collisions, that a considerable higher midrapidity density at the energies of the future supercolliders is obtained from structure functions which behave like $f \sim x^{-1.5}$ and that the increase of the rapidity plateau compared to calculations with "standard" structure functions is mainly due to the contribu-
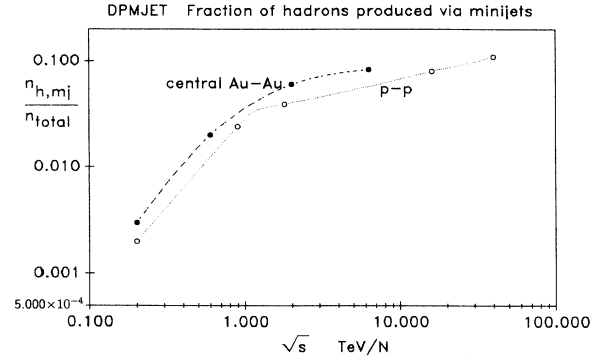
FIG. 7. Fraction of produced hadrons resulting from the minijet component in DPMJET. Open symbols: proton-proton collisions. Solid symbols: Central Au-Au collisions. The lower transverse momentum cutoff for minijets is $p_{\perp \text{thr}} = 3$ GeV/c.

tion of the minijets. As discussed above, to a good approximation $dN^{AA}/dy \propto dN^{pp}/dy$ at midrapidities and therefore this increase of the plateau will also appear in nucleus-nucleus interactions. In this case, nuclear shadowing effects will play a more important role than in the calculations presented here (see next section).

B. Rapidity and pseudorapidity distributions in nucleus-nucleus collisions

We report here on central collisions, where the formation time intranuclear cascade is unimportant. We consider only gold (Au) nuclei as typical heavy projectiles and targets.

The rapidity and pseudorapidity distributions of hadrons in central Au-Au collisions can be understood easily from the Glauber model and the properties of hadron production in hadron-hadron collisions. In Fig. 3 the number of Glauber collisions per nucleon is given as a function of the c.m.s. energy. In central Au+Au collisions at $\sqrt{s} = 6.3$ TeV we get about 1500 elementary nucleon-nucleon interactions. The rapidity plateau in hadron-hadron collisions at this energy is about dN/dy $(y=0)=4-5$; therefore, we expect in the central region of the central Au-Au collisions a rapidity plateau of 6000–7500. This is approximately what we find in the Monte Carlo calculation.

In Fig. 8 we present the rapidity distribution of identified hadrons produced in central Au-Au collisions at $\sqrt{s} = 6.3$ TeV/N according to DPMJET. In Fig. 9 we present the pseudorapidity distributions in central Au-Au collisions at energies from $\sqrt{s} = 20$ GeV/N to 6300 GeV/N. The plateau is found to rise much faster with energy than in hadron-hadron collisions. The reasons for this fast rise are (i) the rise of the elementary nucleon-nucleon input cross section in the Glauber model leading to a rise of the number of collisions N and (ii) the rising fraction of sea-sea chains which cease to be suppressed kinematically with rising energy. In Fig. 10 we give for some energies two rapidity distributions in central Au-Au collisions. One distribution is without nuclear shadowing
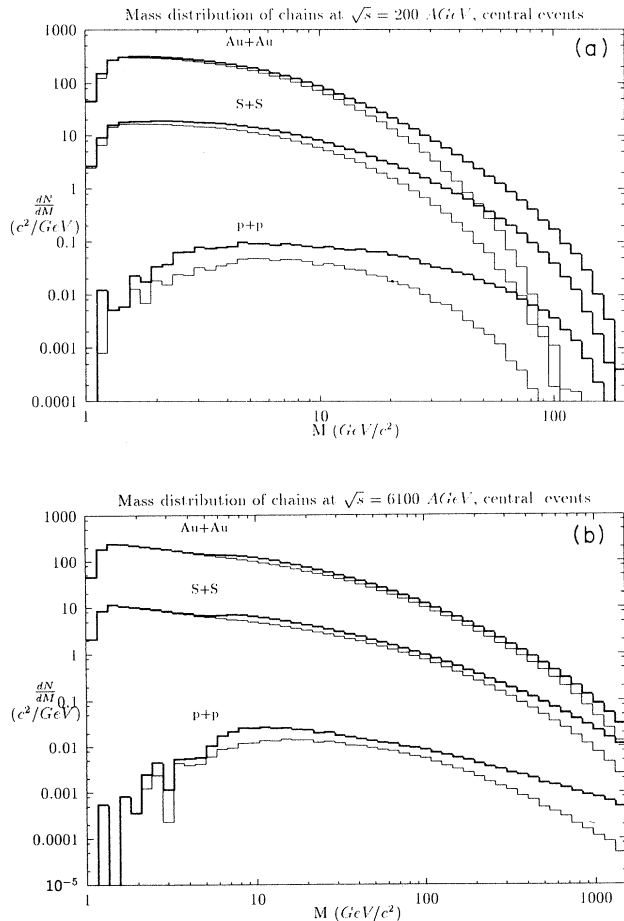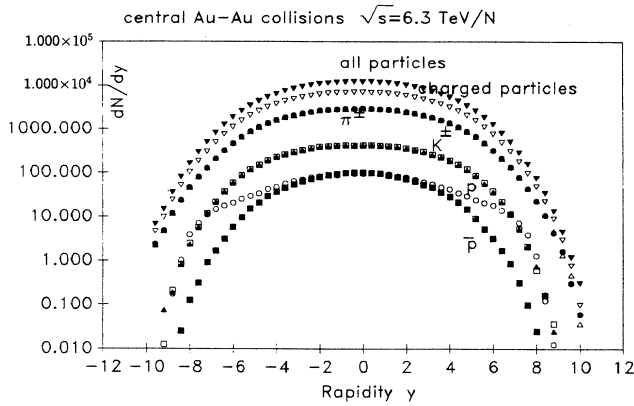

FIG. 6. Chain mass distribution of all (thick lines) and sea-sea (thin lines) chains in $p+p$ and central $S+S$ and Au+Au collisions. (a) $\sqrt{s} = 200$ GeV per nucleon-nucleon. (b) $\sqrt{s} = 6100$ GeV per nucleon-nucleon.

FIG. 8. Rapidity distribution of identified hadrons produced in central Au-Au collisions at $\sqrt{s} = 6.3$ TeV/N according to DPMJET.

FIG. 10. Rapidity distribution of charged particles produced in central Au-Au collisions at $\sqrt{s} = 200$ GeV/N (RHIC), 2000 GeV/N, and 6300 GeV/N (LHC). Solid symbols: Minijets without nuclear shadowing. Open symbols: Minijets with nuclear shadowing according to Eq. (2.5).

of minijets (solid symbols); in the second distribution nuclear shadowing is taken into account according to Eq. (2.5). In contrast with what was found in [25], the differences between both curves are negligible. In our model with a supercritical Pomeron most of the rise of the plateau is still due to the production of soft multiple chains in each elementary collision. Even when about 50% of the minijets are suppressed by the nuclear shadowing (see also the following section), the effect on the total multiplicity and multiplicity density remains small. In [25], a critical Pomeron is used and all the rise of the rapidity plateau in the elementary collisions is due to minijet production; therefore, nuclear shadowing has an enormous effect on the multiplicity density in nucleus-nucleus collisions.

C. Average transverse momenta as a function of pseudorapidity

Average transverse momenta of produced hadrons rise with the collision energy mainly due to the gradual rise of the minijet cross section. Minijets are mainly produced
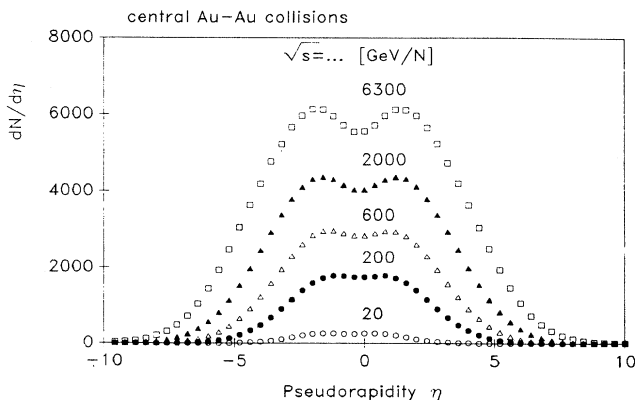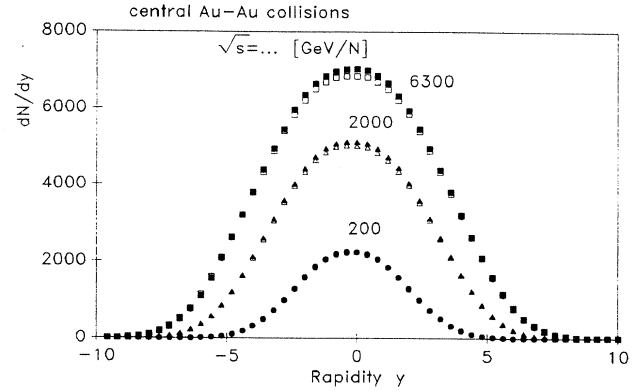
in the central pseudorapidity region; therefore, the average transverse momenta rise strongest in the central region. At larger pseudorapidities the transverse momenta decrease due to kinematics.

In hadron-hadron collisions, the observation of average transverse momenta rising with the multiplicity density in the central rapidity region [1] can very well be understood from the minijet production point of view [6]. DTUJET reproduces the observed $\langle p_\perp \rangle$-multiplicity correlation. In Fig. 11 we present the average transverse momenta of charged particles as a function of pseudorapidity in central Au-Au collisions at energies $\sqrt{s} = 20-6300$ GeV/N. However, it is known that transverse momenta in nuclear collisions are even bigger than in nucleon-nucleon interactions due to the Cronin effect [34]. We plan to incorporate the Cronin effect into our model. This will lead to an increase of the average transverse momenta in most of the rapidity regions against Fig. 11.
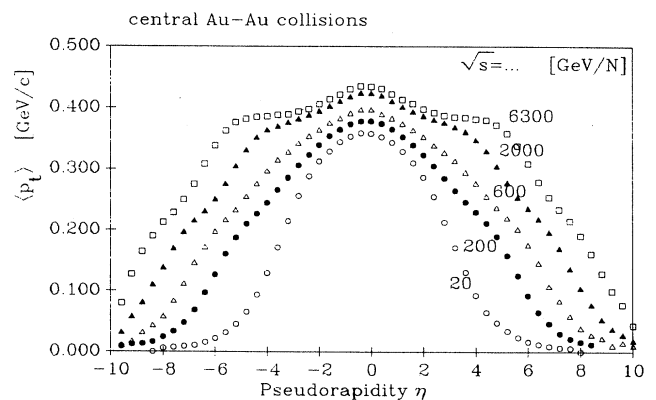

FIG. 9. Pseudorapidity distribution of charged particles produced in central Au-Au collisions at different energies according to DPMJET.

FIG. 11. Average transverse momenta of charged particles as function of the pseudorapidity η for central Au-Au collisions at $\sqrt{s} = 20-6300$ GeV/N. Calculated with DPMJET.
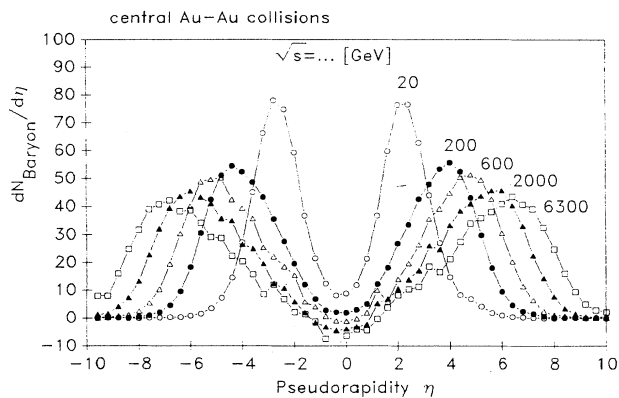
FIG. 12. Pseudorapidity distribution of baryons (sum of all kinds of baryons minus sum of all kinds of antibaryons) in central Au-Au collisions at energies $\sqrt{s} = 20$–6300 GeV/N. Calculated with DPMJET.

D. Baryon stopping

In Fig. 12 we present the baryon multiplicity density as a function of pseudorapidity for central Au-Au collisions at $\sqrt{s} = 20$–6300 GeV/N. At $\sqrt{s} = 20$ GeV/N we find still some finite baryon density in the central region; but starting at energies reached at RHIC DPMJET predicts a growing baryon-free region in the central region of the collision.

In our model, even if the independent production and fragmentation of hadronic chains would not break down, one step is missing so far; this is the (formation zone) cascade of produced hadrons. This step will be implemented in the future. It remains to be seen whether the baryon-free region survives this final state hadron cascade.

IV. THE PARTONIC (MINIJET) COMPONENT TO THE HADRONIC ENERGY DENSITY IN CENTRAL HEAVY-ION COLLISIONS

Two components of the energy density can be calculated separately within our model.

(1) The first component is the hadronic energy density. In this component we collect the energy in the form of hadronic resonances and we assume that these resonances are born after our formation time. This component has been studied in detail in a recent paper [10]. At RHIC and the LHC we find energy densities well in the region where the formation of a quark-gluon plasma is expected.

(2) The second component is the energy density of partons (minijets) resulting from semihard collisions. Only partons which can have further interactions in an explicit parton cascade are included. This component becomes important only at energies reached at LHC. However, the number of minijets depends crucially on the structure function used and the $p_\perp$ cutoff. This is the component which we will study here.

In the conventional DPM the colorless strings between the partons which have participated in hard or semihard primary nucleon-nucleon interactions are fragmented independently. In the TeV energy range of the proposed

Large Hadron Collider a very dense system of such partons may be produced and the independent string fragmentation may fail. In Table II we summarize the average number of hard partons in central Au+Au collisions at $\sqrt{s} = 6.3$ TeV per nucleon pair as obtained from our model using the standard structure functions MRS-1 for $p_\perp$ cuts of 1, 2, and 3 GeV/c. In the second column of Table II we give the results taking into account nuclear shadowing effects.

If we forget for the moment the slow and long-range hadronization process, we can consider these patrons as free particles (at least in the first time after the interaction) moving on straight lines. Indeed, further collisions between the partons are possible. This secondary parton cascade will be studied in more detail in a separate paper. Here we only calculate the energy density carried by the produced minijet component.

The uncertainty of the longitudinal position of a given parton is proportional to its x fraction, $\Delta z = a/x$. If we require that the partons with the smallest possible x value $x_{\min} = 4(p_\perp^{\text{cutoff}})^2/s$ (due to the $p_\perp$ cut) are smeared over $\Delta r = 1$ fm/c, then $a = x_{\min} \Delta r$. According to this consideration we adopt the following space-time picture for the semihard component of the nucleus-nucleus interactions: At time $t = 0$ we consider the incoming nuclei as a collection of partons with momentum fractions $x_i^{p,t}$ and with the transverse coordinates $\mathbf{b}_i$ of their mother nucleons and with a longitudinal coordinate $z_i^{t,p} = \pm z$, z being chosen uniformly between 0 and a/x_i. The number of such partons and the interaction partners are fixed from the Glauber cascade and the DPM. Then the interaction point of the parton i from the projectile and the parton j from the target is given by

$$x = (t, \mathbf{x}) = (z_j^t - z_i^p, \mathbf{b}_i^p + \mathbf{b}_j^t, z_i^p + z_j^t)/2 \ .$$

We introduce instead of the time t and the longitudinal coordinate z the space-time rapidity

$$y = \tfrac{1}{2} \ln[(t+z)/(t-z)]$$

and the eigentime

$$\tau = \sqrt{t^2 - z^2} \ .$$

As a motivation let us mention that in the Bjorken hydrodynamical model [33] all quantities depend only on the space-time rapidity. Now the kinematically possible space-time rapidity region is subdivided in equidistant bins Δy and the four-momenta of the partons are added to the volume elements, in which every parton at this time is. The energy density in the bin i is

TABLE II. Numbers of semihard scattered partons in central Au-Au collisions at LHC energies. $\langle N_{\text{sh}} \rangle$ and $\langle N \rangle$ are the numbers obtained with and without nuclear shadowing.

p_{th} (GeV/c)	$\langle N_{\text{sh}} \rangle$	$\langle N \rangle$
1	12 910	18 155
2	3039	5320
3	1041	1783

$$\epsilon_i(\tau) = \sqrt{p_i^2(\tau)}/(F\tau\Delta y) \ ,$$

where F is the transverse area of the volume element and $p_i(\tau)$ is its total four-momentum at eigentime τ. We have checked that the energy densities ϵ_i do not depend on the bin size for $\Delta y < 0.5$. In Figs. 13 and 14 we present the energy density of the minijet component at eigentimes $\tau = 1$ fm/c and $\tau = 2$ fm/c, respectively. The upper histograms show the results without nuclear shadowing, the lower with shadowing. As can be seen in the figures, the nuclear shadowing reduces the density of the hard partons considerably. Furthermore, the energy density depends crucially on the $p_\perp$ cut in contrast with the results for the final state hadrons.

V. SUMMARY AND CONCLUSIONS

In the present paper we have studied particle production in nucleus-nucleus collisions in the limit of high energies and heavy nuclei. In Refs. [6,8] good agreement

with existing experimental data was found in the case of $p\bar{p}$ collisions up to the highest available energy of $\sqrt{s} = 1.8$ TeV. The generalization to the case of nucleus-nucleus interactions in the framework of Glauber formalism was shown to work well in the limit of low energies and light projectiles (see Refs. [9,10,12]). Therefore it may be expected that deviations from our predictions would be a clear signal for *new physics*.

(1) String interactions. An important feature of our model is the idea of independent string fragmentation. Going to higher energies and nuclear number the transverse string density grows rapidly and reaches the value of $\simeq 40$ fm^{-2} in central Au+Au collisions at the energy reached at LHC (in central $S+S$ collisions at $\sqrt{s} = 20A$ GeV the transverse chain density is $\simeq 2$). It is difficult to believe that in this case the chains would really fragment independently. In Refs. [16,35] the influence of string-string fusion on the particle spectra was studied and it is
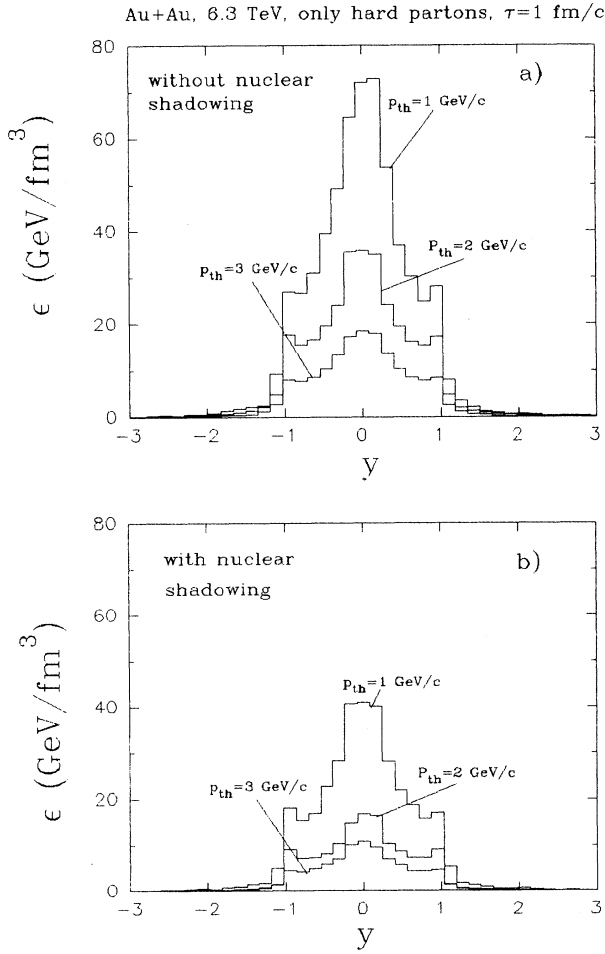

FIG. 13. The energy density of the minijet component in central Au+Au collisions at $\sqrt{s} = 6.3$ TeV at eigentime $\tau = 1$ fm/c. The three curves correspond to $p_\perp$ cuts of 1, 2, and 3 GeV/c, respectively. In the lower histograms the hard Pomeron numbers are sampled taking into account nuclear shadowing effects.
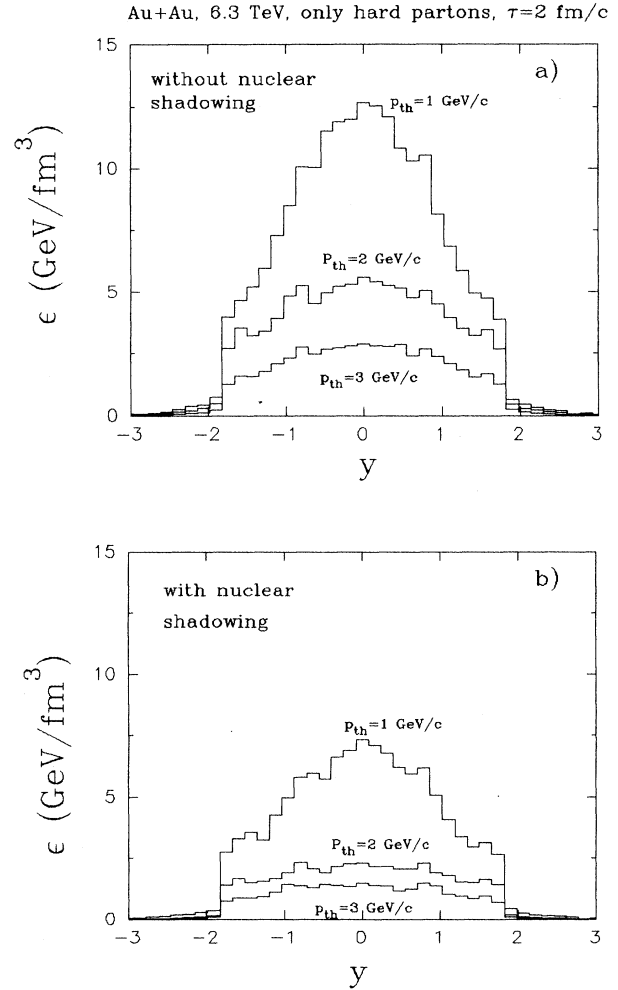
FIG. 14. The energy density of the minijet component in central Au+Au collisions at $\sqrt{s} = 6.3$ TeV at eigentime $\tau = 2$ fm/c. The three curves correspond to $p_\perp$ cuts of 1, 2, and 3 GeV/c, respectively. In the lower histograms the hard Pomeron numbers are sampled taking into account nuclear shadowing effects.

expected that this string interaction will lower the rapidity plateau.

(2) *Interactions of secondary hadrons.* Generally it can be expected that interactions between the produced particles, which are not taken into account in our calculations, may produce additional transverse flow, i.e., additional rise of the average transverse momentum and further changes in the spectra of final state hadrons.

(3) *Interactions of the partons.* Interactions between the partons at the ends of the hard chains may also change the spectra of the observed particles. Because of these interactions the quark-gluon plasma may be formed if their time scale allow thermal equilibrium to be reached before the densities of the system fall below the critical density.

Finally we want to note the importance of the precise value of the soft Pomeron intercept $\alpha'(0)$. In our calculation we have used $\alpha'(0) > 1$ (supercritical soft Pomeron). This can be motivated with the results of Ref. [5], where including the diffractive cross sections into the fit procedure, no consistent fit could be found with a critical $[\alpha'(0) = 1]$ soft Pomeron. Thus, in our model the rise of the total nucleon-nucleon cross section is due both to the rise of the soft Pomeron cross section and the rise of the minijet cross section. In models where a critical soft Pomeron is incorporated [4,25], the main rise of the rapidity plateau results from minijets. Hence, their predictions are very sensitive to nuclear corrections to the structure functions.

ACKNOWLEDGMENTS

APPENDIX: DETAILS ABOUT THE TWO-COMPONENT DUAL PARTON MODEL

1. Input cross sections for the DPM unitarization scheme

The soft input cross section σ_s is parametrized according to the supercritical Pomeron with parameters as determined by Capella, Tran Thanh Van, and Kwiecinski [3]:

$$\sigma_s = g^2 s^\Delta \tag{A1}$$

with

$$g^2 = 40.8 \text{ mb} \tag{A2}$$

and the Pomeron intercept

$$\Delta = \alpha(0) - 1 . \tag{A3}$$

The Pomeron trajectory is given by

$$\alpha(t) = \alpha(0) + \alpha' t \tag{A4}$$

with

$$\alpha(0) = 1.076 , \quad \alpha' = 0.24 \text{ GeV}^{-2} . \tag{A5}$$

The calculation and sampling of hard constituent scattering cross sections within our model was described

in detail in [7]. In order to remain in the region where the QCD perturbation theory is valid, we use for the minijet component a low $p_\perp$ cutoff $p_\perp^{\text{cutoff}}$. The outcome of the model should not depend on the exact value of this cutoff; we use the values $p_\perp^{\text{cutoff}} = 2$ GeV/c and $p_\perp^{\text{cutoff}} = 3$ GeV/c. In the energy region of hadron colliders up to $\sqrt{s} = 1$ or 2 TeV the results are indeed nearly independent of the cutoff.

In Table I we give calculated values of the hard cross sections σ_h for the cutoffs of 2 and 3 GeV/c. This table can be used to determine σ_h at other energies by interpolation.

2. Unitarization of the cross sections

A few words about the unitarization procedure: We start from input cross sections in the impact parameter representation (eikonal) and describe a model with only soft and hard input cross sections. We introduce the soft cross section

$$\chi_s(B,s) = \frac{\sigma_s}{8\pi b_s} \exp\left[-\frac{B^2}{4b_s} \right] , \tag{A6}$$

and the hard cross section

$$\chi_h(B,s) = \frac{\sigma_h}{8\pi b_h} \exp\left[-\frac{B^2}{4b_h} \right] . \tag{A7}$$

We use the slopes $b = 3.52$ GeV^2 and $b_h = b$, $b_s = b_{TP} = b_L = b + \alpha' \ln s / 1$. The normalization of these cross sections is given by

$$\int 2\chi_i(B,s) d^2B = \sigma_i . \tag{A8}$$

In Figs. 1 and 2 we give Pomeron exchange graphs, which correspond to these cross sections.

Let us now consider the exclusive cross sections with l_c cut soft Pomerons and m_c cut hard Pomerons. These are the cross sections, which we need for the construction of inelastic events in the dual parton model. In the eikonal model we have

$$\sigma(l_c, m_c, B, s) = \frac{(2\chi_s)^{l_c}}{l_c!} \frac{(2\chi_h)^{m_c}}{m_c!} e^{-2\chi(B,s)} \tag{A9}$$

with

$$\chi(B,s) = \chi_s(B,s) + \chi_h(B,s) . \tag{A10}$$

We obtain the unitarized hadronic cross sections as follows. The inelastic cross section

$$\sigma_{\text{inel}} = \int d^2B \sum_{l_c + m_c \geq 1} \sigma(l_c, m_c, B, s)$$

$$= 2\pi \int_0^\infty B \, dB (1 - e^{-2\chi(B,s)}) . \tag{A11}$$

The total cross section is given by

$$\sigma_{\text{tot}} = 4\pi \int_0^\infty B \, dB (1 - e^{-\chi(B,s)}) . \tag{A12}$$

Notice that this last formula is only approximate, since we have neglected the real parts of the eikonal.

[1] UA1 Collaboration, G. Arnison *et al.*, Phys. Lett. **118B**, 167 (1982).

[2] A. Capella, U. Sukhatme, C-I Tan, and J. Tran Thanh Van, Orsay Report No. LPTHE 92-38, 1992 (unpublished).

[3] A. Capella, J. Tran Thanh Van, and J. Kwiecinski, Phys. Rev. Lett. **58**, 2015 (1987).

[4] L. Durand and H. Pi, Phys. Rev. Lett. **58**, 303 (1987).

[5] R. Engel, F. W. Bopp, D. Pertermann, and J. Ranft, Phys. Rev. D **46**, 5192 (1992).

[6] P. Aurenche, F. W. Bopp, A. Capella, J. Kwiecinski, M. Maire, J. Ranft, and J. Tran Thanh Van, Phys. Rev. D **45**, 92 (1992); F. W. Bopp, A. Capella, J. Ranft, and J. Tran Thanh Van, Z. Phys. C **51**, 99 (1991).

[7] K. Hahn and J. Ranft, Phys. Rev. D **41**, 1463 (1990).

[8] D. Pertermann, F. W. Bopp, and J. Ranft, Z. Phys. C **54**, 683 (1992).

[9] H. J. Möhring and J. Ranft, Z. Phys. C **52**, 643 (1991).

[10] I. Kawrakov, H. J. Möhring, and J. Ranft, Z. Phys. C **56**, 115 (1992).

[11] H.-J. Möhring and J. Ranft, Leipzig Report No. UL-HEP 92-02, 1992 (unpublished).

[12] H.-J. Möhring, J. Ranft, A. Capella, and J. Tran Thanh Van, this issue, Phys. Rev. D **47**, 4150 (1993).

[13] S. Yu. Shmakov, V. U. Uzhinskii, and A. M. Zadorozhnyi, Comput. Phys. Commun. **54**, 125 (1989).

[14] S. Ritter and J. Ranft, Acta Phys. Pol. B **11**, 259 (1980); S. Ritter, Z. Phys. C **6**, 27 (1982); Comput. Phys. Commun. **31**, 393 (1984).

[15] J. Ranft, Phys. Rev. D **37**, 1842 (1988); Z. Phys. C **43**, 439 (1989).

[16] C. Merino, C. Pajares, and J. Ranft, Phys. Lett. B **276**, 168 (1992); H.-J. Möhring, J. Ranft, C. Merino, and C. Pajares, this issue, Phys. Rev. D, **47**, 4146 (1993).

[17] See *Quark-Gluon Plasma*, edited by R. C. Hwa (World Scientific, Singapore, 1990).

[18] K. Hänssgen and S. Ritter, Comput. Phys. Commun. **31**, 411 (1984).

[19] R. Castaldi and G. Sanguinetti, Annu. Rev. Nucl. Part. Sci. **35**, 351 (1985).

[20] Particle Data Group, J. J. Hernández *et al.*, Phys. Lett. B **239**, 1 (1990).

[21] B. L. Combridge, J. Kripfganz, and J. Ranft, Phys. Lett. **70B**, 234 (1977).

[22] A. D. Martin, R. G. Roberts, and W. J. Stirling, Phys. Lett. B **206**, 327 (1988); Phys. Rev. D **37**, 1161 (1988).

[23] V. A. Abramovski, V. N. Gribov, and O. V. Kancheli, Yad. Fiz. **18**, 595 (1971) [Sov. J. Nucl. Phys. **18**, 308 (1971)].

[24] EM Collaboration, J. Ashman *et al.*, Phys. Lett. B **202**, 603 (1988); M. Arneodo *et al.*, *ibid*. **211**, 493 (1988).

[25] X.-N. Wang and M. Gyulassy, Phys. Rev. D **44**, 3501 (1991).

[26] A. Mueller and J. Qiu, Nucl. Phys. **B268**, 477 (1986).

[27] L. L. Frankfurt and M. I. Strikman, Phys. Rep. **160**, 235 (1988).

[28] K. G. Boreskov and A. B. Kaidalov, Yad. Fiz. **48**, 575 (1988) [Sov. J. Nucl. Phys. **48**, 367 (1988)]; A. Capella, C. Pajares, and A. V. Ramallo, Nucl. Phys. **B241**, 75 (1984).

[29] WA80 Collaboration, H. Gustafson, in *Proceedings of the XXIst International Symposium on Multiparticle Dynamics*, Wuhan, China, 1991, edited by L. Liu and Y. Wu (World Scientific, Singapore, 1992).

[30] WA80 Collaboration, R. Albrecht *et al.*, Z. Phys. C **45**, 529 (1990).

[31] L. Landau and I. Pomeranchuk, Dokl. Akad. Nauk SSR **92**, 535 (1953); **92**, 734 (1953).

[32] L. Stodolski, in *Proceedings of the Vth International Colloquium on Multiparticle Reactions* (Oxford University, Oxford, 1975), p. 577.

[33] J. D. Bjorken, Phys. Rev. D **27**, 140 (1983).

[34] J. W. Cronin *et al.*, Phys. Rev. D **11**, 3105 (1975); J. P. Blaizot and A. Krzywicki, *ibid*. **46**, 246 (1992).

[35] C. Pajares, Phys. Lett. B **258**, 461 (1991); in *Quark Gluon Plasma Signatures*, Proceedings of the International Workshop, Strasbourg, France, 1991, edited by V. Bernard *et al.* (Editions Frontieres, Gif-sur-Yvette, 1991); M. Braun and C. Pajares, Nucl. Phys. **B390**, 542 (1993); **B390**, 559 (1993); N. Amelin, in *Proceedings of the XIIth International Symposium on Multiparticle Dynamics*, Santiago de Compostela, 1992 (World Scientific, Singapore, in press).